



Build-up of macroscopic eigenstates in a memory-based constrained system

Matthieu Labousse, Stéphane Perrard, Yves Couder, Emmanuel Fort

► To cite this version:

Matthieu Labousse, Stéphane Perrard, Yves Couder, Emmanuel Fort. Build-up of macroscopic eigenstates in a memory-based constrained system. *New Journal of Physics*, 2014, 16, pp.113027. 10.1088/1367-2630/16/11/113027 . hal-01084731

HAL Id: hal-01084731

<https://hal.science/hal-01084731>

Submitted on 19 Nov 2014

HAL is a multi-disciplinary open access archive for the deposit and dissemination of scientific research documents, whether they are published or not. The documents may come from teaching and research institutions in France or abroad, or from public or private research centers.

L'archive ouverte pluridisciplinaire **HAL**, est destinée au dépôt et à la diffusion de documents scientifiques de niveau recherche, publiés ou non, émanant des établissements d'enseignement et de recherche français ou étrangers, des laboratoires publics ou privés.

Build-up of macroscopic eigenstates in a memory-based constrained system

This content has been downloaded from IOPscience. Please scroll down to see the full text.

2014 New J. Phys. 16 113027

(<http://iopscience.iop.org/1367-2630/16/11/113027>)

View [the table of contents for this issue](#), or go to the [journal homepage](#) for more

Download details:

This content was downloaded by: labousse

IP Address: 193.54.87.192

This content was downloaded on 14/11/2014 at 14:22

Please note that [terms and conditions apply](#).

Build-up of macroscopic eigenstates in a memory-based constrained system

M Labousse¹, S Perrard², Y Couder² and E Fort³

¹ Institut Langevin, ESPCI Paristech, CNRS, Pierre and Marie Curie University, 1 rue Jussieu, 75005, Paris, France

² Laboratoire Matière et Systèmes Complexes, Université Paris Diderot 10 rue Alice Domon et Léonie Duquet, 75005 Paris, France

³ Institut Langevin, ESPCI Paristech, CNRS, PSL Research University, 1 rue Jussieu, 75005, Paris, France

E-mail: matthieu.labousse@espci.fr, stephane.perrard@univ-paris-diderot.fr, couder@lps.ens.fr and emmanuel.fort@espci.fr

Received 14 July 2014, revised 3 September 2014

Accepted for publication 19 September 2014

Published 11 November 2014

New Journal of Physics **16** (2014) 113027

doi:[10.1088/1367-2630/16/11/113027](https://doi.org/10.1088/1367-2630/16/11/113027)

Abstract

A bouncing drop and its associated accompanying wave forms a walker. Based on previous works, we show in this article that it is possible to formulate a simple theoretical framework for the walker dynamics. It relies on a time scale decomposition corresponding to the effects successively generated when the memory effects increase. While the short time scale effect is simply responsible for the walker's propulsion, the intermediate scale generates spontaneously pivotal structures endowed with angular momentum. At an even larger memory scale, if the walker is spatially confined, the pivots become the building blocks of a self-organization into a global structure. This new theoretical framework is applied in the presence of an external harmonic potential, and reveals the underlying mechanisms leading to the emergence of the macroscopic spatial organization reported by Perrard *et al* (2014 *Nature Commun.* **5** 3219).

Keywords: memory-based dynamics, Wave self-organization, nonlinear dynamics



Content from this work may be used under the terms of the [Creative Commons Attribution 3.0 licence](https://creativecommons.org/licenses/by/3.0/). Any further distribution of this work must maintain attribution to the author(s) and the title of the work, journal citation and DOI.

1. Introduction

Complex systems often require building several hierarching levels of description. This raises fundamental questions in high-dimensional systems about the relevant amount of information needed to characterize them [2–4]. Here, we investigate the case of a strongly nonlinear dynamics in which its apparent complexity can be tremendously reduced, giving way to the surprising quantification of its observables.

An experimental situation has revealed that a *walker* [5], this macroscopic association of a bouncing drop and its accompanying wave, exhibits a dynamics sufficiently complex to reproduce at an unusual scale, a quantum-like effect such as diffraction through submarines slits [6], tunnelling [7], Zeeman-like splitting [8], wave-like statistics in cavities [9], or else a Landau level analogue [10–12]. Perrard *et al* [1] investigated the case where the system, a droplet set on a vertically-vibrated bath and self-propelled by its accompanying wave, is subjected to a two-dimensional (2D) harmonic central potential of natural frequency $\omega/2\pi$. They singled out elementary paths on which the full dynamics can be decomposed. In particular, they showed that the phase space of the dynamics can be projected on a state diagram (n, m) . The integer n is associated with the time-average orbit extension and m the quantized mean angular momentum, satisfying $m \in \{-n, -n + 2, \dots, n - 2, n\}$ reminiscent of the quantum selection rules. In the current paper, we investigate the mechanism responsible for the emergence of these macroscopic eigenstates.

As in the previous reported experiments, we consider a millimetric drop of silicon oil bouncing on a bath oscillating vertically at a frequency $f_0 = 80$ Hz, with an acceleration $\gamma = \gamma_m \cos(2\pi f_0 t)$. The coalescence is prevented by the permanent presence of a thin film of air between the drop and the bath [13–16]. In addition, above a critical Faraday acceleration threshold γ_F , the surface is unstable at a frequency $f_0/2$, and standing waves appear spontaneously as initially observed by Faraday [17] and further studied in [18–20] (see the review [21] and references therein). We restrain our study to the case with period doubling at an acceleration amplitude γ_m slightly below the Faraday acceleration threshold, typically $\gamma_F/(\gamma_F - \gamma_m) \sim 0.98$. In this situation, the drop excites parametrically the surface wave, each impact generating a Bessel-like mode centred at the impact point [22, 23]. The surface height h derives from the linear superposition of the elementary contributions of the previous impacts. Each contribution relaxes to the equilibrium over a typical time decay; henceforth the memory time $\tau = MT_F$. This memory parameter M indicates the relevant number of secondary sources contributing to the surface field. $M \sim \gamma_F/(\gamma_F - \gamma_m)$ is tuned by changing the driving acceleration amplitude. Impacts that occurred more than a few M Faraday periods in the past are negligible. Above a critical memory parameter $M_c \sim 3$, the vertical bouncing state is unstable to a horizontal perturbation. The drop lands on an inclined surface and acquires an increment of horizontal momentum proportional to the local slope [10, 23, 24], which initiates a horizontal motion at typical speed ~ 10 mm s⁻¹.

Figure 1 represents typical examples of the wave field and the associated horizontal walker dynamics as the memory increases. For short memory parameter M (see figure 1(a)), the surface field mainly propels the droplet forward at a constant speed. This regime defines the short time scale $\tau_1 \sim T_F$ and the eponymous dynamics. For intermediate memory parameter M (see figure 1(b)), an increasing number of secondary sources can interfere, and semi-local surface field structures can arise. The walker can turn around these structures and reinforce them. We unambiguously call these characteristic wave structures, *pivotal wave structures*. This

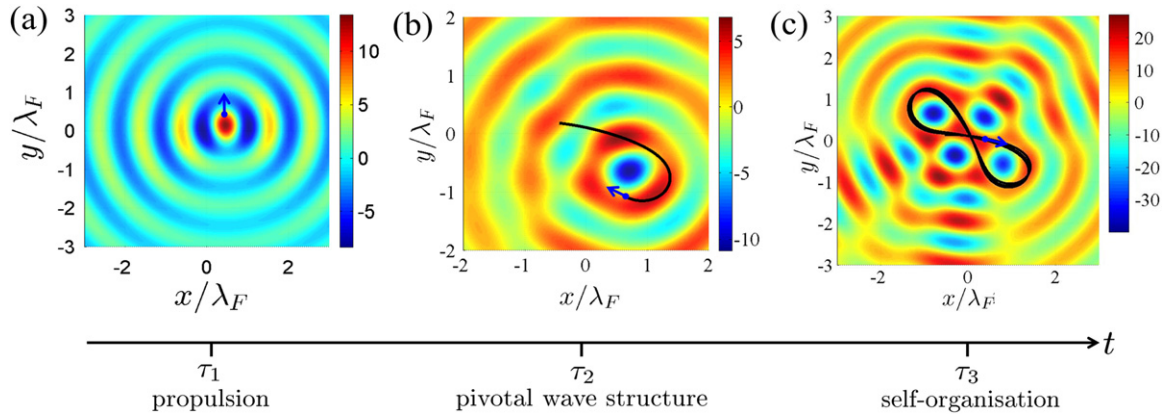


Figure 1. Typical example of a walker dynamics in a harmonic potential (here $(\omega/2\pi = 1.32 \text{ Hz})$ in a natural unit or $(\omega/2\pi = 0.0330)$ in a Faraday period time unit) and the corresponding wave field as the memory increases. In this specific case the time average speed is 7.9 mm s^{-1} . The wave fields are reconstructed from the simulated paths (Fort numerical model [1]). (a) Local structure: memory $M = 9$, the wave field propels the drop. (b) Semi local structure: $M = 19$, some semi local pivotal structures arise. The drop is propelled and guided by a pivotal surface wave field. (c) Global structure: $M = 150$, the drop is now propelled and guided in a fully coherent structure, corresponding to a well-defined organization of the pivotal surface wave field.

phenomenon acts on a typical time scale $\tau_2 \gg \tau_1$ and defines the intermediate time scale dynamics. As the memory is much larger (see figure 1(c)), several reminiscent pivotal fields can coexist, and a global coherent structure emerges from an apparently complex path. It corresponds to a well-defined organization of these pivotal wave structures. This organization acts on a third time scale $\tau_3 \gg \tau_2 \gg \tau_1$ and defines the long time scale dynamics. It indicates a clear separation of time scale, associating with space scale organization of well-defined surface field structures. At long memory, all these time scales interlock, and the effect of each of them can be revealed as the memory parameter increases. The main goal of this paper is to present a theoretical framework in the presence of an attractive potential in the light of this spatio-temporal separation of scales. As it is surprising that this macroscopic wave particle association, when immersed into a harmonic potential, gives rise to a set of attractors with a classical selection rule reminiscent of its quantum counterpart [1], we propose to apply this theoretical framework to explain how such classical attractors emerge.

In the first part, we recall the symmetry properties of the surface field and their consequence on its further time-scale decomposition. In the second part, we formulate the short time dynamics and express it close to the constraint of small speed fluctuations. In the third part, we zoom out a first time, and we add the semi-local wave structure emerging from the pivotal field. The dynamics is described in the Frenet-adapted wave basis and shows that this basis is actually adapted to the translational invariance property of the surface field. We describe how the system evolves with preferred radii of curvature. These pivotal structures constitute the basic units of the dynamics. In the last part, we zoom out once again and see how these pivots interact and organize with each other, which defines the long time dynamics. We show that this self organization emerges from a compromise between two *a priori* incompatible symmetries. The location of the translational-invariant pivotal fields have to account for the rotational-invariant central force.

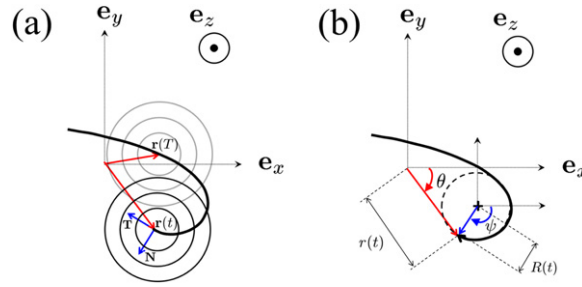


Figure 2. (a) Schematics of the dynamics. The origin of referential $(\mathbf{e}_x, \mathbf{e}_y)$ corresponds to the minimum of energy of the attractive potential. The motion defines the tangential and the normal direction so that (\mathbf{T}, \mathbf{N}) forms a direct basis. The standing wave-field at a given instant t interferes with the remaining standing wave generated in the past (for all past sources so that $T < t$). (b) We define two bases: the polar basis (r, θ) of origin prescribed by the minimum of energy of the attractive potential and the basis (R, ψ) of origin at the instantaneous centre of curvature. R denotes the algebraic radius of curvature.

2. The space-time separation of the field

The theoretical description of the walker dynamics has already been introduced in previous works [5, 10, 15, 22, 24]. The idea of this paper is to use the time scale separation of the dynamics to reduce the complexity of the existing theoretical frameworks. As the drop bounces synchronously with the bath every Faraday period, and the horizontal distance between two impacts is much smaller than the Faraday wavelength, the horizontal dynamics can be approximated by a continuous description [24]

$$\frac{d\mathbf{v}}{dt} = -\gamma\mathbf{v} - C[\nabla h]_{\mathbf{r}(t)} - \left[\frac{\nabla E_p}{m} \right]_{\mathbf{r}(t)} \quad (1)$$

with \mathbf{r} the horizontal drop position and \mathbf{v} its horizontal speed as sketched in figure 2(a). The length scales and time are normalized by $\lambda_F/2\pi$ ($\lambda_F = 4.75$ mm) and the Faraday period T_F ($T_F = 25$ ms). E_p denotes an external attractive potential that will be further specified. The interaction with the surface consists in an apparent friction term $-\gamma\mathbf{v}$ and a coupling with the local slope of the surface field $-C[\nabla h]_{\mathbf{r}(t)}$, the gradient being taken at the drop position at a given time. In principle, the coefficients γ and C can be deduced from the benchmarked Fort's numerical model [1, 6, 10] or from the hydrodynamic model of Moláček *et al* [15, 23]. They are used here as free parameters and further chosen to match the experiments. Evaluating this field at the instantaneous particle position $\mathbf{r}(t)$ yields [10, 24].

$$h(\mathbf{r}, t) = \int_{-\infty}^t \frac{dT}{T_F} J_0(\|\mathbf{r}(t) - \mathbf{r}(T)\|) e^{-(t-T)/M} \quad (2)$$

with J_0 the first order Bessel function, being centred at the point of a past impact $\mathbf{r}(T)$ and felt at $\mathbf{r}(t)$, the current position of the drop. The origin of different time scales arises intrinsically from the surface term. It is typically the time interval required to generate different hierarchies of coherent wave structures. In paragraph 2.1, we first recall symmetry properties of the surface field h and we use them in paragraph 2.2 to separate the different time scales of the dynamics

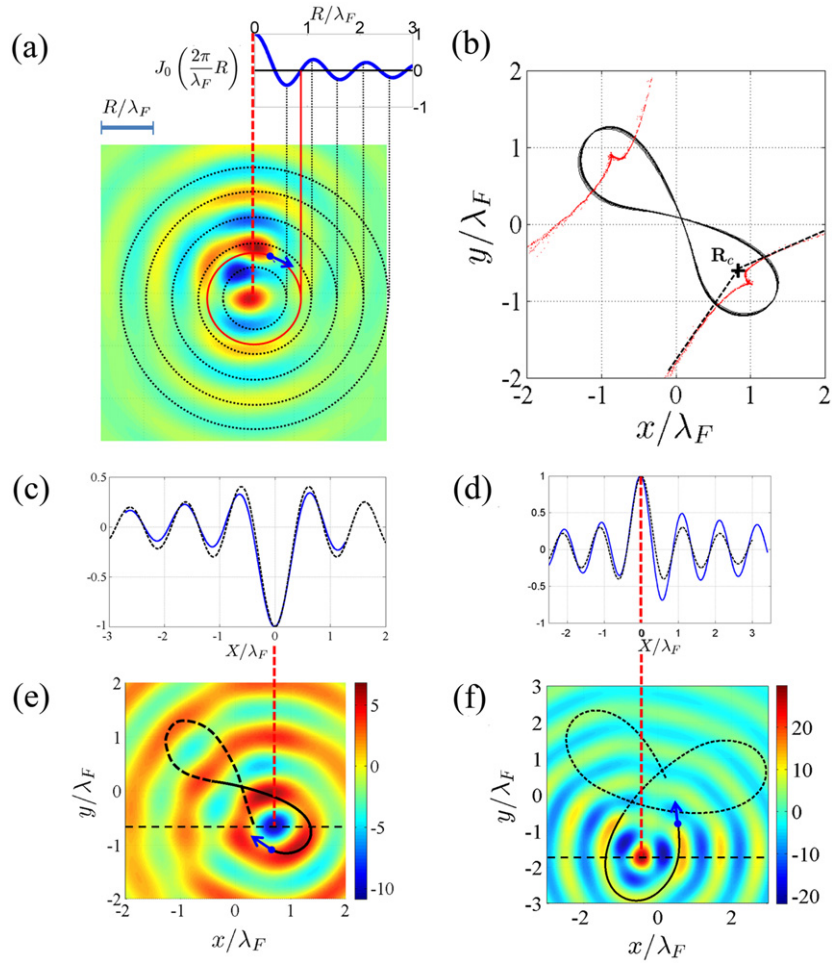


Figure 3. (a) Simulated circular motion $(n,m) = (2,-2)$ at $M = 21$ ([1], supplementary methods) for $\omega/2\pi = 0.023$ (in Faraday period time unit). The position of the drop is indicated by a blue spot and the whole circular motion by the red circle of radius $\approx 0.9\lambda_F$. The circles in black dotted lines correspond to the extrema of the Bessel function of order 0 centred at the origin and plotted in the above sub-figure. The surface field is reconstructed *a posteriori*, owing to equation (2), and is similar to the experimental one. We can separate the surface field into two terms: an intense part, immediately following and propelling the drop and a coherent part resulting from the interference of the secondary sources. (b) Simulated lemniscate motion $(n,m) = (2,0)$ at $M = 21$ [1] for $\omega/2\pi = 0.033$ (in Faraday period time unit). The black line indicates the path followed by the drop. The red points denote the loci of the instantaneous centre of curvature. \mathbf{R}_c denotes the centre of the pivotal field and corresponds to the barycentre of the damped past sources. (c) and (e) Pivotal structure of a lemniscate. (c) In the blue line, the slice of the wave field; in the black line, a centred Bessel function of order 0 of negative amplitude. From \mathbf{R}_c : the symmetry of the efficiently- contributed path is roughly rotational-invariant and generates the surface field corresponding to this symmetry at the leading order. (e) We superpose the reconstructed wave field and the path ($\omega/2\pi = 0.033$ (in Faraday period time unit)). The black line qualitatively indicates the part of the path effectively contributing to the wave field (typically a dimensionless memory curvilinear length $\approx VMT_F/\lambda_F$). As the drop is turning back to the centre, it generates a wave field: a Bessel function of order 0 centred in \mathbf{R}_c . (d) and (f) The pivotal structure of a trefoil $(n,m) = (4,2)$. (d) and (f) are similar to (c) and (e) but for a trefoil ($\omega/2\pi = 0.016$ (in Faraday period time unit)).

2.1. Symmetry properties of the surface field

The dynamics relies on three difference time scales: the propulsion, the semi-local structure, and the global organization. Zooming in on these different dynamical aspects requires developing different tools, particularly in order to describe the surface field.

Being a solution of the two dimensional Helmholtz equation, the local value of the surface field can be decomposed into a polar Bessel eigenfunction $\{f_n(\tilde{r}, \tilde{\theta})\}_{n \in \mathbb{Z}} = \{J_n(\tilde{r})e^{in\tilde{\theta}}\}_{n \in \mathbb{Z}}$, with a free choice in the centre of decomposition. In this sense, the wave field revealed translational-invariant properties. The surface field can be indifferently decomposed onto a Frenet-adapted wave basis $\{f_n^F(t)\}_{n \in \mathbb{Z}} = \{J_n(R(t))e^{in\psi(t)}\}_{n \in \mathbb{Z}}$

$$\begin{cases} h(\mathbf{r}(t), t) = \sum_{n \in \mathbb{Z}} h_n^F f_n^F(t) \\ h_n^F(t) = \langle h | f_n^F \rangle = \int_{-\infty}^t \frac{dT}{T_F} J_n(R(T)) e^{-in\psi(T)} e^{-(t-T)/M} \end{cases} \quad (3)$$

as well as onto a basis of centre adapted to the external potential $\{f_n^{\text{ext}}(t)\}_{n \in \mathbb{Z}} = \{J_n(r(t))e^{in\theta(t)}\}_{n \in \mathbb{Z}}$

$$\begin{cases} h(\mathbf{r}, t) = \sum_{n \in \mathbb{Z}} h_n^{\text{ext}} f_n^{\text{ext}}(t) \\ h_n^{\text{ext}}(t) = \langle h | f_n^{\text{ext}} \rangle = \int_{-\infty}^t \frac{dT}{T_F} J_n(r(T)) e^{-in\theta(T)} e^{-(t-T)/M} \end{cases} \quad (4)$$

The different coordinates are indicated in figure 2(b) and correspond to two different polar bases. In equation (3), the Frenet basis R denotes the instantaneous radius of curvature, while ψ indicates the local polar angle having its origin at the instantaneous centre of curvature. In the central polar basis decomposition (equation (4)), (r, θ) indicates the usual polar coordinates, the origin coinciding with the centre of the external potential. Let us briefly mention that in both equations (3) and (4), no imaginary part is effectively added, and the whole expression remains real.

Equations (3) and (4) are mathematically equivalent and simply correspond to two different viewpoints. The decomposition in the Frenet basis (equation (3)) corresponds to a projection of the local value of the wave field into eigenmodes. This decomposition will be used in section 4 to express the intermediate time scale dynamics. The decomposition onto a central basis reflects the symmetry of the harmonic potential. We will study in paragraph 5 how the pivotal wave structure builds a long term self-organization.

2.2. Time scale decomposition of the surface field

Distinguishing the different time scales of the dynamics requires separating two physical effects taking place at the surface: the propulsion and the construction of an intermediate/long time coherent surface field structure. To highlight the separation of these two physical effects, the path and the surface field corresponding to the circular attractor $(n, m) = (2, 2)$ are shown in figure 3(a). It was obtained from path memory simulations (see [1] supplementary materials). As the memory and the position of each impact are known, the surface field can be numerically reconstructed from equation (2). Two distinct parts of the field can be distinguished in

figure 3(a), the first one, intense, directly following the drop and providing the propulsion, and the second one arising from the constructive interference of the secondary sources left all along the path. This coherent surface field structure has a dominant term reflecting the signature of the rotational symmetry of the path, here $J_0(2\pi R/\lambda_F)$, as emphasized by sub-figure 3(a). The propulsion is short-term acting, while the constructive interference requires a much larger duration to be established. This separation of time scales can be revisited in a theoretical manner, considering the work of Oza *et al* [11] and M Miskin [25] for a circular path of radius r_c of angular speed ω_c . The coupling with the local slope of the surface field $-C \nabla h^{\text{circle}}$ can be theoretically derived, leading to

$$\begin{cases} \partial_T h^{\text{circle}} = -\frac{1}{\omega_c r_c} (1 - J_0^2(r_c)) + \mathcal{O}\left(\frac{1}{(\omega M)^2}\right) & (a) \\ \partial_N h^{\text{circle}} = M J_0(r_c) J_1(r_c) + \mathcal{O}\left(\frac{1}{\omega^2 M}\right) & (b) \end{cases} \quad (5)$$

where ∂_N and ∂_T denote the gradients along the normal and tangential direction to the trajectory. The tangential gradient of the field (equation (5)(a)) becomes independent of the memory M in the long memory limits. It indicates that the propulsion is a short time effect (further indexed st). On the contrary, the growth of the normal gradient (equation 5(b)) with the memory M indicates a longer time effect (further indexed lt). The propulsion slightly depends on the memory at the leading order, as it would be a short-acting effect. On the opposite, it takes at least a few memory times to establish the constructive interferences leading to (equation 5(b)). Guided by this idea, it becomes natural to decompose the field for any path into two parts

$$h = H^{\text{st}} + H^{\text{lt}} \quad (6)$$

and dissociate the propulsive contribution H^{st} from the coherent structure H^{lt} . The short time effect, being mainly propulsive, admits mainly a tangential component and also imposes

$$\partial_N H^{\text{st}} \simeq 0, \text{ hypothesis (a)} \quad (7)$$

As a corollary, the propulsion being a short term action, we define the long term evolution of the field so that it does not contribute anymore to the propulsion, i.e.,

$$\partial_T H^{\text{lt}} = 0, \text{ hypothesis (b)} \quad (8)$$

These two hypotheses impose two constraints, which, should have consequences on the description of the field. The Frenet decomposition of the surface wave (equation (3)) prescribes

$$h(\mathbf{r}, t) = h_0^F f_0^F(t) + \sum_{n \in \mathbb{Z}^*} h_n^F f_n^F(t) = h_0^F J_0(R(t)) + \sum_{n \in \mathbb{Z}^*} h_n^F J_n(R(t)) e^{in\psi(t)}. \quad (9)$$

Seeking in equation (9), the terms having a zero tangential derivative (hypothesis (b)) yields $H^{\text{lt}} = h_0^F f_0^F(t)$. Consequently, we identify $H^{\text{st}} = \sum_{n \in \mathbb{Z}^*} h_n^F f_n^F(t)$. Note that hypothesis (b) can be taken as a definition of H^{lt} . H^{st} contains all the tangential derivatives and is the only one responsible for the propulsion. Section 3 is devoted to this short time scale dynamics and will express $\partial_T H^{\text{st}}$ on its symmetry in speed. But what about hypothesis (a)? As we remain in the short memory regime, the tangential component of the gradient $\partial_T H^{\text{st}}$ dominates its normal

component $\partial_N H^{\text{st}}$ [26]. But is it still valid as we get into a longer memory regime? Section 4 deals with the intermediate time scale dynamics and will investigate how this physical hypothesis stands as we go onto a more complex trajectory.

3. Short time scale dynamics: the propulsion

The income of energy to the drop mediated by H^{st} increases its horizontal momentum. Nevertheless, as the friction starts acting, the drop loses a part of energy, and a dynamical exchange of its energy between the surface field and the drop occurs. This process defines a steady velocity v_0 at which the energy propelling the particle balances its frictional loss of energy. In the regime parameter of interest, this equilibrium speed is a constant of the motion. In the phase space of the dynamics, this constraint defines a manifold in the neighbourhood of which it is convenient to express the dynamics. This constraint on speed contains some of the major non Hamiltonian features of the dynamics in the short memory regime as shown in [26]. Experiments and path-memory simulations of the dynamics in a harmonic potential [1] showed that for a given drop, the mean velocity is a constant of the motion, and the corresponding fluctuations remain small (typically $\sim 10\%$). In the tangential direction, the combined effect of friction and propulsion from the surface $\mathbf{f}(\mathbf{v})$ can be expressed as

$$\mathbf{f}(\mathbf{v}) = -\gamma \mathbf{v} - C \partial_T h \mathbf{T} = -(\gamma v + C \partial_T H^{\text{st}}) \mathbf{T}. \quad (10)$$

Let us mention that only the short term field H^{st} contributes in the tangential direction, as $\partial_T H^{\text{lt}} = 0$. $\mathbf{f}(\mathbf{v})$ is tangential to the trajectory i.e., $\mathbf{f}(\mathbf{v}) = f(v) \mathbf{T}$. The amplitude of the propulsion $f(v)$ must provide v_0 as a fixed point and also is only a function of the amplitude of the speed i.e., $\mathbf{f}(\mathbf{v}) = f(v) \mathbf{T}$. Additionally, $f(v)$, must be odd in v as a complete reverse of the instantaneous of the motion should not break any symmetry in the propulsion, i.e., $f(-v) = -f(v)$. It has been shown [26] that at the smallest order of fluctuations, the propulsion should be written as

$$f(v) = \Gamma v \left(1 - (v/v_0)^2 + \mathcal{O}(v/v_0)^4 \right) \quad (11)$$

Γ is a dimensionless coupling constant which can eventually depends on the memory. Equation (11) known as a Rayleigh-type friction [26–28] can be understood from a dynamical point of view: if v the speed of the particle decreases below v_0 , the density of secondary sources left behind the particle increases the efficiency of the surface field propulsion. On the contrary, if v increases above its set point v_0 , the density of secondary sources decreases, and the propulsion loses some of its efficiency. This asymptotic expansion of the propulsion is similar to the propulsion model of A Boudaoud *et al* [5] and can also be derived from the theoretical works of Oza *et al* [24]. An extension of this model considering the fluctuations in speed has been recently developed by Bush *et al* [29] and shows the importance of these higher order terms in recovering effective mass effects. With the propulsion being expressed in this simple manner, how does the rest of the surface field contribute to the emergence of the intermediate time scale dynamics and of the associated pivotal wave structure?

4. Intermediate time scale dynamics: a semi local organization

In this part we study, the construction of the semi-local wave structures arising at the intermediate time scale. We apply this approach to the lemniscate attractor in the case of a (2D) harmonic potential. First, we propose a qualitative approach. Second, we use the time scale decomposition of the field decomposition (equation (6)) suggested in section 2.2 to rationalize the intermediate time scale dynamics.

4.1. A qualitative approach

Figure 3(b) shows the lemniscate attractor $(n, m) = (2, 0)$ in a stable form obtained by path memory simulations ([1], supplementary methods), similar to the experimental one. We also indicate (in red points) the location of the instantaneous centre of curvature. As shown in [1, 30], the elementary lemniscate path exits under other forms, with an azimuthal drift (typically smaller than $\sim 20^\circ$ per orbital period) or by intermittency in a chaotic regime. In all cases, however, and as shown in figure 3(b), when the particle turns back, its speed is minimal, and its average centre of curvature concentrates in the neighbourhood of the pivotal point, noted \mathbf{r}_c . In figure 3(e), we overdraw in the black curve the part of the path contributing effectively to the pivotal surface structure (typically the M last secondary sources). Then, we plot in the associated figure 3(c) (in the blue line) a slice of the normalized surface field along the x -axis, and in the dashed line a Bessel function of order zero centred at the pivotal point \mathbf{r}_c and of negative and normalized amplitude. The field generated by this elementary pivotal motion is a pivotal field and is well fitted by a Bessel function of order 0, centred in \mathbf{r}_c , which actually defines \mathbf{r}_c . Let us note that the emergence of this structure does not require a large number of secondary sources. The same phenomenon occurs for the trefoil attractor $(n, m) = (4, 2)$, as indicated in the coupled figures 3(d) and (f).

Locally the turn back generates a surface field $\pm J_0(\|\mathbf{r} - \mathbf{R}_c\|)$: the semi local symmetry of the surface field is a signature of the semi local circular symmetry of the path. Qualitatively, the effect of this process is the emergence of a preferred radius of curvature. We now derive theoretically how such structures arise.

4.2. A theoretical approach

The short time scale provides information in the tangential direction short time, and it has been shown in paragraph 3 that the propulsion is mediated by the short time field H^{st} . The rest of field H^{lt} , revealed as the memory increases, is mainly involved in the normal mechanical balance. We now investigate its role in the emergence of the intermediate time scale dynamics and in the construction of the pivotal wave structure.

(\mathbf{T}, \mathbf{N}) denotes the direct Frenet basis (see figure 2(a)). We note $\mathcal{T} = \mathbf{r} \cdot \mathbf{T}$ and $\mathcal{N} = \mathbf{r} \cdot \mathbf{N}$, evolving in time by definition as $\dot{\mathcal{T}} = v + \mathcal{N}v/R$ and $\dot{\mathcal{N}} = -\mathcal{T}v/R$. The mechanical tangential balance yields $\dot{v} = \Gamma v \left(1 - v^2/v_0^2\right) - \partial_{\mathcal{T}} E_p / m$, where $\partial_{\mathcal{T}} E_p$ denotes the tangential projection of the external potential. The normal mechanical balance involves the normal gradient of the field. As $\partial_{\mathcal{N}} H^{\text{st}} = 0$, the normal mechanical balances can be simply written as $v^2/R = -\partial_{\mathcal{N}} E_p / m - C \partial_{\mathcal{N}} H^{\text{lt}}$.

The time decomposition of the surface field indicates that H^{lt} predominantly contributes in the normal direction (hypotheses (b)). It can be expressed as

$$\partial_N H \simeq \partial_N H^{\text{lt}} = h_0^F(t) J_1(R(t)) \quad (12)$$

where h_0^F is the amplitude of the mode $n = 0$. Note that neglecting $\partial_N H^{\text{lt}} \gg \partial_N H^{\text{st}}$ is equivalent to hypothesis (b). This hypothesis relies on the symmetry of the paths we intend to describe: at an intermediate time scale dynamics, the trajectory of the walker is made of a succession of loops. Each loop promotes a dominant local symmetry.

Also, the separation of the time scales in the dynamics enables the modelling of the dynamics by a set of equations

$$\begin{cases} \dot{\mathcal{T}} = v(1 + \mathcal{N}/R) & (a) \\ \dot{\mathcal{N}} = -v\mathcal{T}/R & (b) \\ \dot{h}_0^F = -h_0^F/M + h_0 J_0(R) & (c) \\ \dot{v} = \Gamma v(1 - v^2/v_0^2) - \partial_T E_p/m & (d) \\ v^2/R + \partial_N E_p/m + C J_1(R) h_0^F = 0 & (e) \end{cases} \quad (13)$$

Equations (13(a)) and (13(b)) are kinematic and are consequently always valid. Equation (13(c)) is a differential equation in h_0^F and simply corresponds to a derivation of its integral form (equation (3)). It means that the mode 0 of the Frenet-adapted wave basis evolves in time owing to two distinct contributions: it relaxes over a memory time, and the mode is maintained by the coupling with the drop impacts. Equation 13(c) can be taken as a definition of h_0^F and thus does have to be checked. Equation 13(d) is the momentum balance in the tangential direction and is a direct consequence of the expansion of the dynamics in the neighbourhood of the manifold $\{v = v_0\}$. Equation 13(e) arises from the normal mechanical balance and differs from the others, as no time-derivative is involved. This implicit equation in R actually defines the manifold on which the dynamics evolves.

We apply this approach in the case of a (2D) harmonic potential $E_p = m\omega^2 r^2/2$ of eigenpulsation ω , which leads to

$$\begin{cases} \dot{\mathcal{T}} = v(1 + \mathcal{N}/R) & (a) \\ \dot{\mathcal{N}} = -v\mathcal{T}/R & (b) \\ \dot{h}_0^F = -h_0^F/M + h_0 J_0(R) & (c) \\ \dot{v} = \Gamma v(1 - v^2/v_0^2) - \omega^2 \mathcal{T} & (d) \\ v^2/R + \omega^2 \mathcal{N} + C J_1(R) h_0^F = 0 & (e) \end{cases} \quad (14)$$

Also, the complexity of the dynamics has been reduced to a five dimensional representation $(\mathcal{T}, \mathcal{N}, v, h_0^F, R)$. Can we trust the set of equations 14(d) and (e)? This raises actually two distinct questions. i) Does equation 14(d) model correctly the propulsion? It is interesting to remark that equation 14(d) relies only on speed symmetry arguments, which should remain valid for various memory regimes. The question has already been successfully addressed in the low memory regime by Labousse and Perrard [26], but up till now remains unproven at larger memory. It is the first point we have to check. ii) The simplicity of equation 14(e) actually relies on hypothesis (a) (equation (7)). It is natural to retain only the dominant field symmetry

corresponding to a single pivotal motion, but we have to evaluate *a posteriori* the relevance of such an hypothesis.

The relevance of the set of equation (14) is checked for a lemniscate trajectory in figure 4. Figures 4(a) and (b) respectively, represent the time evolution of the terms involved in the normal and tangential directions (respectively equations 14(d) and (e)). The normal balance is well captured by the equation 14(e) (blue time intervals of figure 4(a)), and the neglected terms $\sim \partial_N H^{\text{st}}$ are well negligible. This justifies hypothesis (a) (see equation (7)). As expected, we also note that the Frenet basis decomposition is not convenient, as the walker moves in a quasi straight line motion (red time intervals of figure 4(a)). Figure 4(b)) shows that the tangential balance is also well captured by the equation 14(d). This paragraph also justifies the physical distinction between a short time field H^{st} , mainly involved in the propulsion, and a long time field H^{lt} , mainly involved in the normal balance. It explains the relevance of the decoupling of the effects of the two distinct time scales, as it can capture the main features of the dynamics.

Figure 4(c) represents a three dimensional (3D) projection of lemniscate attractor $(n, m) = (2, 0)$. The constraint on speed enables a large reduction of dimensions of the phase space in comparison to the integro-differential formulation in [23, 24]. In the integro-differential formulation, the wave field stores an infinite number of degrees of freedom. Provided the fluctuations of speed remain small, a large number of these dimensions can be reduced in a resulting propulsion force (equation (11)) for a large range of memory parameters.

It is useful to study some particular cases of equation (14) to further analyse the consequences of the speed constraint. A first particularly interesting case is the simplest fixed point $v^* = v_0$. It induces $\mathcal{T}^* = 0$ from 14(d) then $\dot{\mathcal{N}}^* = 0$ from 14(b), $\mathcal{N}^* = -R^*$ from 14(a), and, finally, $h_0^{F*} = MJ_0(R^*)$, which corresponds to a circular attractor. The constraint

$$\left(\left(v_0/R^* \right)^2 - (\omega)^2 \right) R^* + CMJ_1(R^*)J_0(R^*) = 0 \quad (15)$$

is multi-valued, as several R^* can satisfy this equation in the high memory limit. The term $\delta = (v_0/R^*)^2 - (\omega^*)^2$ corresponds to a mismatch of frequency between the one arising from the external harmonic potential ω and the natural frequency v/R prescribed by the surface field. They are not necessarily equal, which is a signature of the difference of symmetry between the surface field force and the external force: this set of equations could provide a simplified theoretical framework to study the transitions to the low-dimensional chaotic regimes reported by Perrard *et al* [30]. We recover the condition $J_0(R^*)J_1(R^*) = 0$ in the long memory limit, which gives rise to a quantization of the radius of curvature [1, 10–12, 25, 31].

Another interesting limit case arises when there exists a strong mismatch between the centre of curvature and the origin of the external force $\mathcal{N}/R \ll 1$. Equation 14(d) shows that any spread of difference of speed from its set point induces a retroaction from the term $v(1 - v^2/v_0^2)$. Nevertheless, the coupling to the external potential may induce a non-stationary solution in speed. Indeed, provided $\mathcal{N}/R \ll 1$, time-derivating equation 14(d) leads to $\ddot{v} + \Gamma\dot{v}(1 - 3v^2/v_0^2) + \omega^2v = 0$ and provides a self oscillation of speed (Van der Pol type). These fluctuations of speed would make a straight line motion unstable to any transverse fluctuations. This instability of the straight line motion is observed in harmonic potential [1, 26] in the reported parameter regimes.

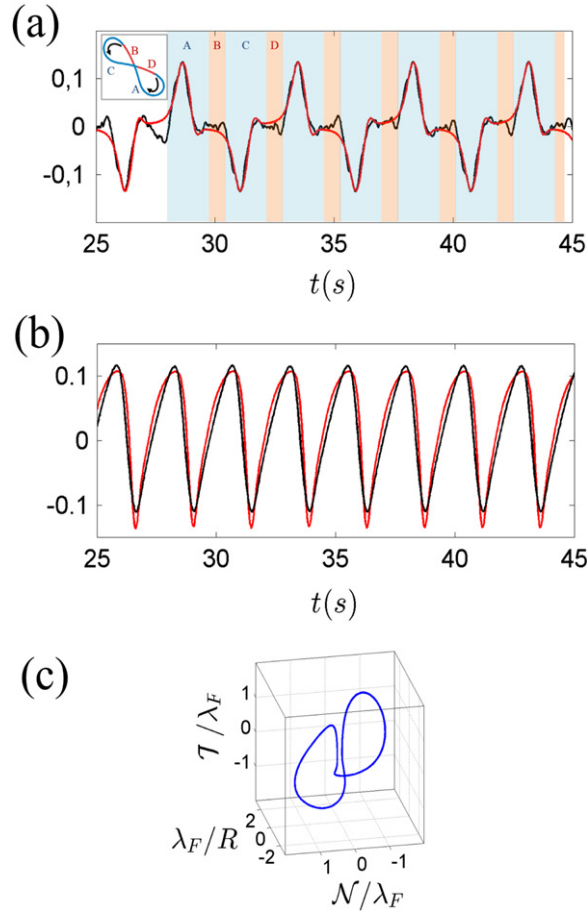


Figure 4. Verification of equation (14) for a lemniscate extracted from the Fort numerical model ($\omega/2\pi = 0.033$ (in Faraday period time unit), $M = 21$). The time and length scales are expressed in natural units. (a) Normal balance from simulation results: in the black line $-CJ_1(2\pi R/\lambda_F)h_0^F$ with $C = 1.40 \text{ m s}^{-2}$ ($C = 0.18$ in dimensionless units), in the red line $v^2/R + \omega^2\mathcal{N}$. The blue time intervals (A,C) indicate a good theoretical prediction of equation 14(e) and correspond to the build up of a pivotal field. The red time intervals (B,D) correspond to the parts of the path that do not adequately fit with 14(e). The insert is the simulated path (see figure 3(b)) and links the time intervals (A,B,C,D) to their corresponding portion of the path. (b) Tangential balance from simulation results: in the black line $\dot{v} + \omega^2\mathcal{T}$, in the red line $\Gamma v(1 - v^2/v_0^2)$ with $\Gamma = 35.0 \text{ s}^{-1}$ ($\Gamma = 0.875$ in dimensionless units), and $v_0 = \sqrt{\langle v^2 \rangle} \simeq 7.9 \text{ mm s}^{-1}$ (or $v_0 = 4.2 \times 10^{-2}$ in dimensionless units). Fluctuations of speed are of 17%. (c) Projection of the in the dimensionless representation (λ_F/R , \mathcal{N}/λ_F , \mathcal{T}/λ_F).

This paragraph focused on the intermediate time scale dynamics. We adopted a point of view adapted to the symmetry of the wave field by choosing to develop the surface field into a Frenet-adapted wave basis. It enables us to separate a short time effect, the propulsion, and an intermediate time effect, the tendency of the dynamics to build a pivotal field, and the emergence of preferred radii of curvature. What will happen to these pivotal structures at the long time scale dynamics?

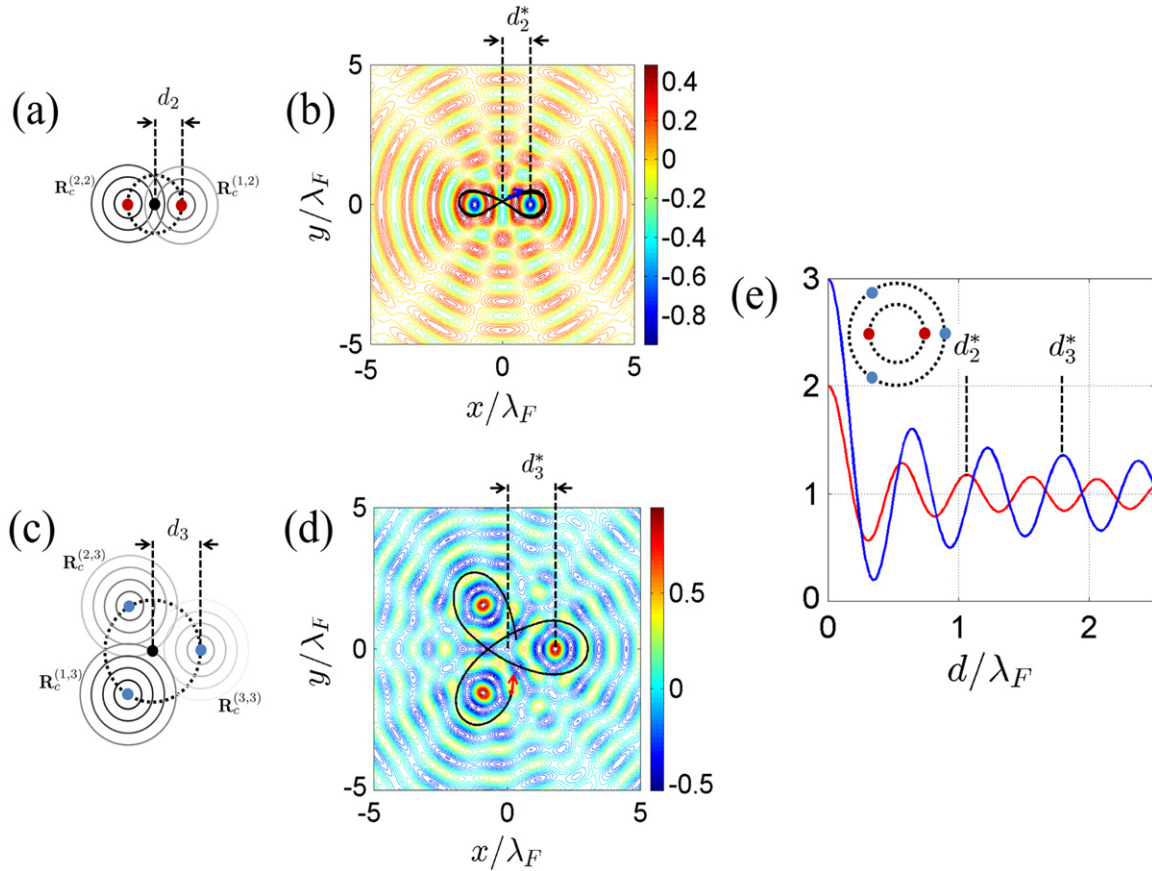


Figure 5. (a) Sketch of the interaction between two pivotal fields. The pivotal points (two red dots) are diametrically opposed on a circle of radius d_2 . The black dot indicates the centre of the harmonic potential. (b) Superposition of two pivotal fields $\mathcal{H}_2 = -(J_0(\|\mathbf{r} - \mathbf{R}_c^{(1,2)}\|) + J_0(\|\mathbf{r} - \mathbf{R}_c^{(2,2)}\|))$ and the associated path with $d_2 = \|\mathbf{R}_c^{(1,2)}\| = \|\mathbf{R}_c^{(2,2)}\|$. Here is chosen a field with $d_2 = d_2^*$. The lemniscate path is identical to figure 3(e). (c) Sketch of the interaction between three pivotal fields. The pivotal points (three blue dots) are $2\pi/3$ equally spaced on a circle of radius d_3 . The black dot indicates the centre of the harmonic potential. (d) Superposition of three pivotal fields $\mathcal{H}_3 = J_0(\|\mathbf{r} - \mathbf{R}_c^{(1,3)}\|) + J_0(\|\mathbf{r} - \mathbf{R}_c^{(2,3)}\|) + J_0(\|\mathbf{r} - \mathbf{R}_c^{(3,3)}\|)$ and the associated path, with $d_3 = \|\mathbf{R}_c^{(1,3)}\| = \|\mathbf{R}_c^{(2,3)}\| = \|\mathbf{R}_c^{(3,3)}\|$. Here, is chosen a field with $d_3 = d_3^*$. The trefoil path is identical to figure 3(f). (e) Evolution of $I_2(d_2)$ (red line) and $I_3(d_3)$ (blue line) with d . Here, d is common notation for d_2 or d_3 .

5. Long time scale dynamics: the global organization of the pivots

We zoom out once again in the scales of time and observe the dynamics at a longer time scale. The memory is thus long enough to store several pivotal structures in the wave field. These pivotal structures should interact via the walker's trajectory. One would also expect to feel the effect of the central force and of its relating symmetry. With the exception of the circular attractor, how can the construction of the pivotal field be compatible with the axisymmetry of the (2D) central harmonic potential?

Perrard *et al* show that the lemniscates and the trefoil attractors have quantized extensions. Consequently, the location of these pivotal points should be well defined, meaning that they

adopt a particular position in space. We propose a simple geometrical approach to justify this quantization. Each about-turn generates a Bessel function centred at its associated pivotal wave structure $J_0(\|\mathbf{r} - \mathbf{R}_c^{(k,n)}\|)$. n indicates the number of the pivotal point: $n = 2$ for the lemniscate and $n = 3$ for the trefoil; $k = 1, \dots, n$ denote the k th pivotal points. We sketched in figure 5(a), the position of the pivotal points $(\mathbf{R}_c^{i,2})_{i=1,2}$ of a lemniscate. They are diametrically opposed on a circle of radius d_2 . We superpose on figure 5(b) a numerical lemniscate path to a field made of the superposition of two pivotal fields, each of them centred on a pivotal point $(\mathbf{R}_c^{i,2})_{i=1,2}$. Figures 5(c) and (d) are similar to figures 5(a) and (b), except for a trefoil, with three pivotal points $(\mathbf{R}_c^{i,3})_{i=1,2,3}$ that are $2\pi/3$ equally spaced.

Figure 5(b) indicates the contour line of the superposition of two pivotal fields $\mathcal{H}_2 = -(J_0(\|\mathbf{r} - \mathbf{R}_c^{(1,2)}\|) + J_0(\|\mathbf{r} - \mathbf{R}_c^{(2,2)}\|))$, and figure 5(d) shows the superposition of three pivotal fields $\mathcal{H}_3 = J_0(\|\mathbf{r} - \mathbf{R}_c^{(1,3)}\|) + J_0(\|\mathbf{r} - \mathbf{R}_c^{(2,3)}\|) + J_0(\|\mathbf{r} - \mathbf{R}_c^{(3,3)}\|)$. To estimate the spatial coherence between the successive pivotal fields, we compute the interfering quantity related to the superposition of n pivotal fields.

$$I_n(d_n) = \frac{1}{A_n} \iint \mathcal{H}_n^2 dS = \frac{1}{A_n} \iint \left(\sum_{k=1}^n J_0(\|\mathbf{r} - \mathbf{R}_c^{(k,n)}\|) \right)^2 dS. \quad (16)$$

where $d_n = \|\mathbf{R}_c^{(k,n)}\|$ is the distance between the k th pivotal point and the centre of symmetry of the trajectories. The integration is realized numerically in a large ($20\lambda_F \times 20\lambda_F$) but finite centred surface domain. It is normalized by A_n , a quantity independent of d which makes I_n independent on the domain of integration.

$$A_n = \frac{1}{n} \iint \left(\sum_{k=1}^n J_0(\|\mathbf{r}\|) \right)^2 dS. \quad (17)$$

figure 5(e) shows the evolution of I_n with d_n and presents optima of interfering conditions for quantized distances $d_n = d_n^*$. In particular, it predicts $d_2^* = 1.08\lambda_F$ for the lemniscate and $d_3^* = 1.80\lambda_F$ for the trefoil, respectively. It is in good agreement with the pivotal points of the lemniscate in figure 3(e) ($1.015\lambda_F$), and of the trefoil in figure 3(f) ($1.79\lambda_F$). The well-defined position of the pivotal points are a signature of the symmetry of the external potential. It suggests reconstructing the equation of motion in a basis adapted to the harmonic central potential. It would imply that $\mathcal{H}_n(d^*)$ corresponds to a local maximum of overlapping with the central wave basis $\{f_n^{\text{ext}}(t)\}_{n \in \mathbb{Z}} = \{J_n(r(t)e^{in\theta(t)})\}_{n \in \mathbb{Z}}$. Figure 5(f) presents other maxima, but they are not observed experimentally. For low distance d_n , these states are in competition with the circular attractors. This geometrical approach only demonstrates how the pivotal fields are organized between each other but did not account for the dynamical stability.

6. Conclusion

We investigated the walker dynamics subjected to an attractive potential. The main goal of the current paper was to show that the dynamics lies on three time scales, unveiled as the memory parameter increases. At a short time scale, the accompanying surface wave simply propels the drop. At an intermediate time scale, the appearance of a coherent wave structure that we call the pivotal field induces motion with preferred radii of curvature. This elementary wave pattern

give rise to a well-defined motion and can be seen as an elementary block of motion. The long time scale dynamics assembles these elementary pivotal fields to maximize their mutual interferences. The external potential imposes its own symmetry, which a given disposition of the pivotal fields has to account for.

We applied our theoretical framework to a particular case of the (2D) harmonic potential. We explained how these three time scales and relating spatial self-organizations are interlocked. The mechanism provides a new rule of construction for the macroscopic eigenstates reported in [1].

The research of coherent structures is a common technique in complex systems, such as fully developed turbulent flows. In this case, the details of the dynamics do not really matter, and much of the information is stored in a much simpler structure that leads to a hierarchy in the description of the complexity. In the current article, the details of the reported dynamics are forgotten, as they contribute to the emergence of higher order structures. One can reason from a ‘dynamics’ point of view but will be rapidly limited as the complexity of description increases tremendously. One can also sacrifice some details of the dynamics and adopt a description at another time scale. In this limit, the problem is reduced to a self-organization of the elementary wave patterns. The useful amount of information (said differently, the apparent dimensions of the system), depends here on the time scale of the description. In the current object of study, it explains why the dynamics, apparently complex and chaotic, can be reduced to its attractors, which can be simply defined by two integers and called eigenstates.

Acknowledgements

The authors thank Marc Miskin, John Bush Ruben Rosales, and Anand Oza for useful discussions. This research is supported by the AXA Research Fund and the French Agence Nationale de la Recherche, through the project ‘ANR Freeflow’, LABEX WIFI (Laboratory of Excellence ANR-10-LABX-24), within the French Program ‘Investments for the Future’ under reference ANR-10-IDEX-0001-02 PSL.

References

- [1] Perrard S, Labousse M, Miskin M, Fort E and Couder Y 2014 Self-organization into quantized eigenstates of a classical wave driven particle *Nature Commun.* **5** 3219
- [2] Farmer J D 1982 Chaotic attractors of an infinite-dimensional dynamical system *Phys. D* **4** 366–93
- [3] Takens F 1981 Detecting strange attractors in turbulence *Dynamical Systems and Turbulence, Warwick 1980 (Lecture Notes in Mathematics vol 898)* (Berlin: Springer) pp 366–81
- [4] Wolf A, Swift J B, Swinney H L and Vastano J A 1985 Determining lyapounov exponents from a time series *Phys. D* **16** 285–317
- [5] Couder Y, Protière S, Fort E and Boudaoud A 2005 Dynamical phenomena: walking and orbiting droplets *Nature* **437** 208
- [6] Couder Y and Fort E 2006 Single-particle diffraction and interference at macroscopic scale *Phys. Rev. Lett.* **97** 154101
- [7] Eddi A, Fort E, Moisy F and Couder Y 2009 Unpredictable tunneling of a classical wave-particle association *Phys. Rev. Lett.* **102** 240401
- [8] Eddi A, Moukhtar J, Perrard S, Fort E and Couder Y 2012 Level splitting at macroscopic scale *Phys. Rev. Lett.* **108** 264503

- [9] Harris D M, Moukhtar J, Fort E, Couder Y and Bush J W M 2013 Wavelike statistics from pilot-wave dynamics in a circular corral *Phys. Rev. E* **88** 011001
- [10] Fort E, Eddi A, Boudaoud A, Moukhtar J and Couder Y 2010 Path-memory induced quantization of classical orbits *Proc. Natl Acad. Sci. USA* **107** 17515–520
- [11] Oza A U, Harris D M, Rosales R R and Bush J W M 2014 Pilot-wave dynamics in a rotating frame: on the emergence of orbital quantization *J. Fluid Mech.* **744** 404–29
- [12] Harris D M and Bush J W M 2013 Droplets walking in a rotating frame: from quantized orbits to multimodal statistics *J. Fluid Mech.* **739** 444–64
- [13] Protière S, Boudaoud A and Couder Y 2006 Particle wave association on a fluid interface *J. Fluid Mech.* **554** 85–108
- [14] Terwagne D, Gilet T, Vandewalle N and Dorbolo S 2008 A drop spectroscopy *Phys. Mag.* **30** 161–8
- [15] Moláček J and Bush J W M 2013 Drops bouncing on a vibrated bath *J. Fluid Mech.* **727** 582–611
- [16] Moláček J and Bush J W M 2012 A quasi-static model of a drop impact *Phys. Fluids* **24** 127103
- [17] Faraday M 1831 On the forms and states of fluids on vibrating elastic surfaces *Philos. Trans. R. Soc. London* **121** 319–40
- [18] Benjamin T B and Ursell F 1954 The stability of the plane free surface of liquid in vertical periodic motion *Proc. R. Soc. London A* **225** 505–15
- [19] Douady S 1990 Experimental study of the Faraday instability *J. Fluid Mech.* **221** 383–409
- [20] Douady S and Fauve S 1988 Pattern selection in Faraday instability *Europhys. Lett.* **6** 221–6
- [21] Miles J and Henderson D 1990 Parametrically forced surface waves *Annu. Rev. Fluid. Mech.* **22** 143–65
- [22] Eddi A, Sultan E, Moukhtar J, Fort E, Rossi M and Couder Y 2011 Information stored in faraday waves: the origin of a path memory *J. Fluid Mech.* **674** 433–63
- [23] Moláček J and Bush J W M 2013 Drops walking on a vibrating bath: towards a hydrodynamic pilot-wave theory *J. Fluid Mech.* **727** 612–47
- [24] Oza A U, Rosales R R and Bush J W M 2013 A trajectory equation for walking droplets: hydrodynamic pilot-wave theory *J. Fluid Mech.* **737** 552–70
- [25] Miskin M 2012 Private communications
- [26] Labousse M and Perrard S 2014 Non hamiltonian features of a classical pilot-wave dynamics *Phys. Rev. E* **90** 022913
- [27] Rayleigh J W 1877 *The Theory of Sound* (London: Macmillan)
- [28] Erdmann U and Ebeling W 2005 On the attractors of two dimensionnal rayleigh oscillators including noise *Int. J. Bifurcation Chaos* **15** 3623–33
- [29] Bush J W M, Oza A U and Moláček J 2014 *J. Fluid Mech.* **755** R7
- [30] Perrard S, Labousse M, Fort E and Couder Y 2014 Chaos driven by interfering memory *Phys. Rev. Lett.* **113** 104101
- [31] Oza A U, Wind-Willassen Ø, Harris D M, Rosales R R and Bush J W M 2014 Pilot-wave hydrodynamics in a rotating frame: exotic orbits *Phys. Fluids* **26** 082101